AGU PUBLICATIONS

Water Resources Research

RESEARCH ARTICLE
10.1002/2015WR017961

Representing spatial variability of forest snow: Implementation of a new interception model

D. Moeser[1,2], G. Mazzotti[1], N. Helbig[1], and T. Jonas[1]

[1]WSL Institute for Snow and Avalanche Research SLF, Davos Dorf, Switzerland, [2]Forest Ecology, Institute of Terrestrial Ecosystems, Department of Environmental Sciences, Swiss Federal Institute of Technology ETH, Zurich, Switzerland

Key Points:
- Framework to integrate a new interception model into snowmelt models
- Model resolves spatial distribution of under-canopy snow in heterogeneous forests
- Model performs well under a broad range of canopy openness

Correspondence to:
D. Moeser,
moeser@slf.ch

Citation:
Moeser, D., G. Mazzotti, N. Helbig, and T. Jonas (2016), Representing spatial variability of forest snow: Implementation of a new interception model, *Water Resour. Res.*, *52*, doi:10.1002/2015WR017961.

Received 5 AUG 2015
Accepted 31 DEC 2015
Accepted article online 7 JAN 2016

Abstract A new interception model was integrated in a snowmelt model and for the first time the spatial variability of forest snow was effectively represented due to the inclusion of new forest structure metrics. The model was tested at 1273 field points surrounding Davos, Switzerland, that feature an extremely wide range of canopy and forest structure. The behavior of the new model was compared against a widely applied interception model. Due to the inclusion of novel forest structure parameters (mean distance to canopy and total gap area) in the new model, simulated interception mimicked the horizontal layout of canopy structure, while the standard interception model yielded fairly homogeneous interception estimations even under highly heterogeneous canopy conditions. The large variance of estimated interception between points using the new model translated into significant effects on under-canopy snow water equivalent and snow depth. Precipitation conditions were also analyzed, and further differences between the models were related to storm intensity. In climates characterized by large storm events, the new interception model provides significantly higher interception estimations (i.e., lower under-canopy snow) than the standard model, whereas in climates characterized by small storms events, the new model yields lower interception estimations (i.e., higher under-canopy snow) in areas with moderately sized to large canopy gaps.

1. Introduction

Forests directly impact the snow accumulation and melt cycles over large areas. In the Northern Hemisphere, 20% of the seasonal snow cover occurs within forested regions, which accounts for 17% of the total terrestrial winter water budget [*Guntner et al.*, 2007]. Primarily, the presence and structure of forest canopy affects the under-canopy snow distribution due to snow interception on the canopy and processes that lead to the release of intercepted snow, such as snow unloading and sublimation. Besides major implications for the water budget, the interplay of these mechanisms also affects albedo and the related energy transfer processes in forest regions.

Intercepted snow estimates range from 0 to 80% of the total annual snowfall within forested areas and the longer intercepted snow remains in the canopy, the more sublimation can occur [*Martin et al.*, 2013; *Moeser et al.*, 2015b; *Montesi et al.*, 2003; *Storck et al.*, 2002]. Due to this, the spatially heterogeneous nature of interception leads to equally heterogeneous sublimation rates, which vary from 0 to 50% of the total annual snowfall in forested areas [*Essery and Pomeroy*, 2001; *Essery et al.*, 2003; *Hedstrom and Pomeroy*, 1998; *Lundberg and Halldin*, 2001].

Many studies that have focused on forest-snow interactions, with initial research starting over 100 years ago. To date there have been four synthesis reviews of these efforts, which all highlight the complex nature of forest-snow interactions as well as sometimes disparate interception measurement methods and results [*Bunnell et al.*, 1985; *Friesen et al.*, 2014; *Lundberg and Halldin*, 2001; *Varhola et al.*, 2010b]. In 2007, an assessment of the skill of current snowmelt models that include representations of canopy-snow interactions (Snow model inter-comparison project – SNOWMIP2) was undertaken [*Essery et al.*, 2009; *Rutter et al.*, 2009]. Within this project, not only was no best fit model found for the sites included in the study, but model performance showed much lower consistency for forested areas than for open areas. These findings underscore the sometimes overly simplistic representation of canopy structure in the underlying processes. All the models in SNOWMIP2 that utilized a snow interception module integrated canopy closure (CC) and/or leaf area index (LAI) to parameterize the canopy. However, prior studies showed that field points that have

the same LAI or CC can have different large-scale canopy structures, such as open areas surrounding these points [*Moeser et al*., 2015a,2015b]. Furthermore, the importance of the greater forest structure has also been highlighted as a major factor dictating the under-canopy SWE accumulation patterns and timing of snow melt [*Golding and Swanson*, 1986; *Lopez-Moreno and Latron*, 2008; *Lopez-Moreno and Stähli*, 2008; *Troendle and Meiman*, 1986; *Varhola and Coops*, 2013; *Varhola et al*., 2010a; *Veatch et al*., 2009; *Winkler and Moore*, 2006; *Winkler et al*., 2005].

Despite the large amount of research on the interactions between forest canopy and snow, few studies have attempted to quantify this in the form of a mechanistically relevant interception model that can be integrated in a snowmelt model. *Storck* [2000] created a model for maximum interception capacity based on data from the Pacific Norwest of the US in the form of a temperature-based stepwise function that integrated LAI, and combined this with a constant interception efficiency (percentage of precipitation that is intercepted) multiplier which was first applied and tested by *Andreadis et al*. [2009]. *Hedstrom and Pomeroy* [1998] developed an interception model based on data from a boreal forest and were among the first to include canopy parameters (CC and LAI) and combined this approach with an interception efficiency function based on precipitation. This interception model has been widely used in the majority of the SNOWMIP2 models and is hereafter referred to as the "standard model." Despite the fact that this is a major step forward, the model did not integrate snow bridging or branch bending, which were formalized in past studies [*Satterlund and Haupt*, 1967; *Schmidt and Gluns*, 1991] by a sigmoidal function of interception efficiency (i.e., interception divided by precipitation). Instead, the model used an exponential decay function that reduces interception efficiency with increasing precipitation during a storm.

In order to (1) better represent the interplay between local canopy characteristics (LAI, CC) and the greater canopy structure and (2) provide an interception efficiency function valid in Norwegian spruce forests, *Moeser et al*. [2015b] developed a new interception model. It utilized canopy closure, total gap area, and mean distance to canopy (see section 2.3) to characterize the canopy and the structure of the surrounding forest. It also integrated a sigmoidal interception efficiency function to represent snow bridging that reflects an initial exponential increase (representing snow bridging) of the efficiency to a maximum, and a subsequent efficiency decrease (representing branch bending). Here, this new interception model is integrated in a snowmelt model. Since the interception model was initially formulated as a function of total interception during a storm event it necessitated adaptations to function appropriately within a dynamic, discrete-time model.

The principal goal of this study was to (A) implement the new interception model in an existing snowmelt model, the Factorial Snow Model (FSM) [*Essery*, 2015], at hourly time steps under a range of canopy and forest structure conditions. The subsequent analysis will show, (A-1) how the inclusion of forest scale canopy metrics (total gap area, mean distance to canopy) better accounts for the heterogeneous nature of under-canopy snow, (A-2) how the use of a sigmoidal interception efficiency distribution affects the interception and under-canopy snow estimations, and (A-3) how this new model deviates from a model that features a standard parameterization of interception when used in different precipitation regimes.

2. Methods

2.1. Overview of the FSM Model

The Factorial Snow Model (FSM) is a simplified multimodel approach currently under development and evolved from the JIM (Jules Investigation Model) modeling framework [*Essery et al*., 2013]. The JIM framework is an energy balance-based snowmelt model that allows for three different parameterizations of seven snow processes, yielding 1701 potential model configurations [*Essery et al*., 2013]. From this and other projects no specific configuration was found to yield optimal snow mass simulations, however a group of configurations provided consistently better performances than others [*Magnusson et al*., 2015]. Thus, these groupings were used to guide the configurations of FSM for the present study. The FSM includes two potential parameterizations for five snow properties and processes: albedo, heat conduction, snow density, turbulent fluxes and liquid water content (for details see *Essery* [2015]). None of the parameterizations for these snow processes are new, and similar guiding equations can be found in several models, including CLASS [*Clark et al*., 2015a,2015b,2015c; *Verseghy*, 1990], CLM [*Oleson et al*., 2010], HTESSEL [*Dutra et al*., 2010], ISBA [*Boone*, 2009; *Douville et al*., 1995], JULES [*Best et al*., 2011], MOSES [*Cox et al*., 1999], and UEB [*Mahat and*

Tarboton, 2014; *Tarboton and Luce*, 1996]. The primary function of the FSM model is not necessarily for forecasting but rather for providing a framework to evaluate how new parameterizations function within a comprehensive snow model. For this study, we implemented a canopy module in FSM with two possible parameterizations for canopy snow interception and affiliated processes (unloading and sublimation), where one parameterization used the standard *Hedstrom and Pomeroy* [1998] interception model and the second parameterization used the *Moeser et al*. [2015b] interception model (see Section 2.5 for details). Both interception parameterizations used the same unloading and sublimation modules in order to directly test the sensitivity of the new interception model against the standard model. The addition of these two interception parameters (to the existing parameterizations for each of the 5 snow properties and processes, as outlined above) led to an increase from 32 to 64 model configurations.

Hourly meteorological driving data of incoming shortwave radiation - ISWR (W m^{-2}), incoming longwave radiation - ILWR (W m^{-2}), snowfall rate - S_f (kg $m^{-2}s^{-1}$), rainfall rate - R_f (kg $m^{-2}s^{-1}$), air temperature - T_a (K), relative humidity - RH (%),wind speed - V (m s^{-1}), and surface air pressure - P_s (Pa) were needed in order to run the model. In order to utilize the interception configurations, GF, LAI, mean distance to canopy (m), and total gap area (m^2) were also needed at each point where the model was run.

2.2. Field Areas

Snow data from five field areas and two open areas at three elevation bands were utilized for this study (Figure 1). These areas were part of a long-term forest snow research initiative set up in Fall 2012 by the WSL Institute for Snow and Avalanche Research (SLF). Each of the five areas had a size of 2500 m^2 and were chosen for study due their heterogeneous canopy cover which included larger scale forest properties such as forest openings. The stands are dominated by Norway spruce (*Picea abies*) and range in height from 0.5 to 45 m. The field areas have minimal terrain shading influence and low to no surface slopes. In each field area, a sampling grid was set up containing 276 points that were labeled and surveyed. Two open areas were also used (also part of the SLF forest snow research project) for comparison with the under-canopy measurements (see Figure 1 for a map outlining the location of the field areas as well as aerial LiDAR representations of the field areas). For more detailed information regarding the field sites, cf. *Moeser et al*. [2014].

2.3. Snow Measurements

Snow depth (SD) and snow water equivalent (SWE) measurements were taken during the 2012/2013 and 2013/2014 winter seasons after all storm events (which had greater than 15 cm of SD in the open). SD measurements were taken at all sample grid points both in and outside the forest (1480 points in total). Total SWE was taken at twelve points per forested field area, and at two points per open field area.

Prior studies have utilized a variety of methods to quantify canopy interception, including weighing tree experiments [*Hedstrom and Pomeroy*, 1998; *Nakai et al*., 1994, 1999; *Pomeroy et al*., 1998; *Satterlund and Haupt*, 1967; *Schmidt and Gluns*, 1991; *Storck et al*., 2002; *Suzuki and Nakai*, 2008], Gamma Ray attenuation [*Calder*, 1991], time lapse photography [*Bründl et al*., 1999; *Kobayashi*, 1987; *Nakai et al*., 1999; *Tennyson et al*., 1974] and weighing lysimeters [*Andreadis et al*., 2009; *Storck et al*., 2002]. However, because of the large logistics effort required for these methods, no point-based data have been collected over large scales to date (see *Friesen et al*. [2015] for a detailed overview of measurement techniques). Thus, a method to indirectly measure interception was utilized. Snow interception was measured when specific ground and meteorological preconditions were prevailing: (1) solid crust on snow prior to storm, (2) no interception on trees prior to storm, and (3) low to no wind redistribution during storm events. Nine storms in the two winter seasons met these conditions. In these cases, SD of the new snow on top of the crust was measured. Interception was determined as the difference between the depth of the newly fallen snow in the open areas and the SD in the forest at each grid point. Finally, all field points that were in positions that could have hindered the quality of the measurement were removed from the data set. This included points on top of stumps, on logs, in depressions or in areas where trees fell during the sampling campaign. This reduced the number of measurement points from 1480 to 1276.

The interception data were converted to water equivalent (SWE) using the fresh snow density model derived from the *US Army Corps of Engineers* [1956] by *Hedstrom and Pomeroy*[1998].

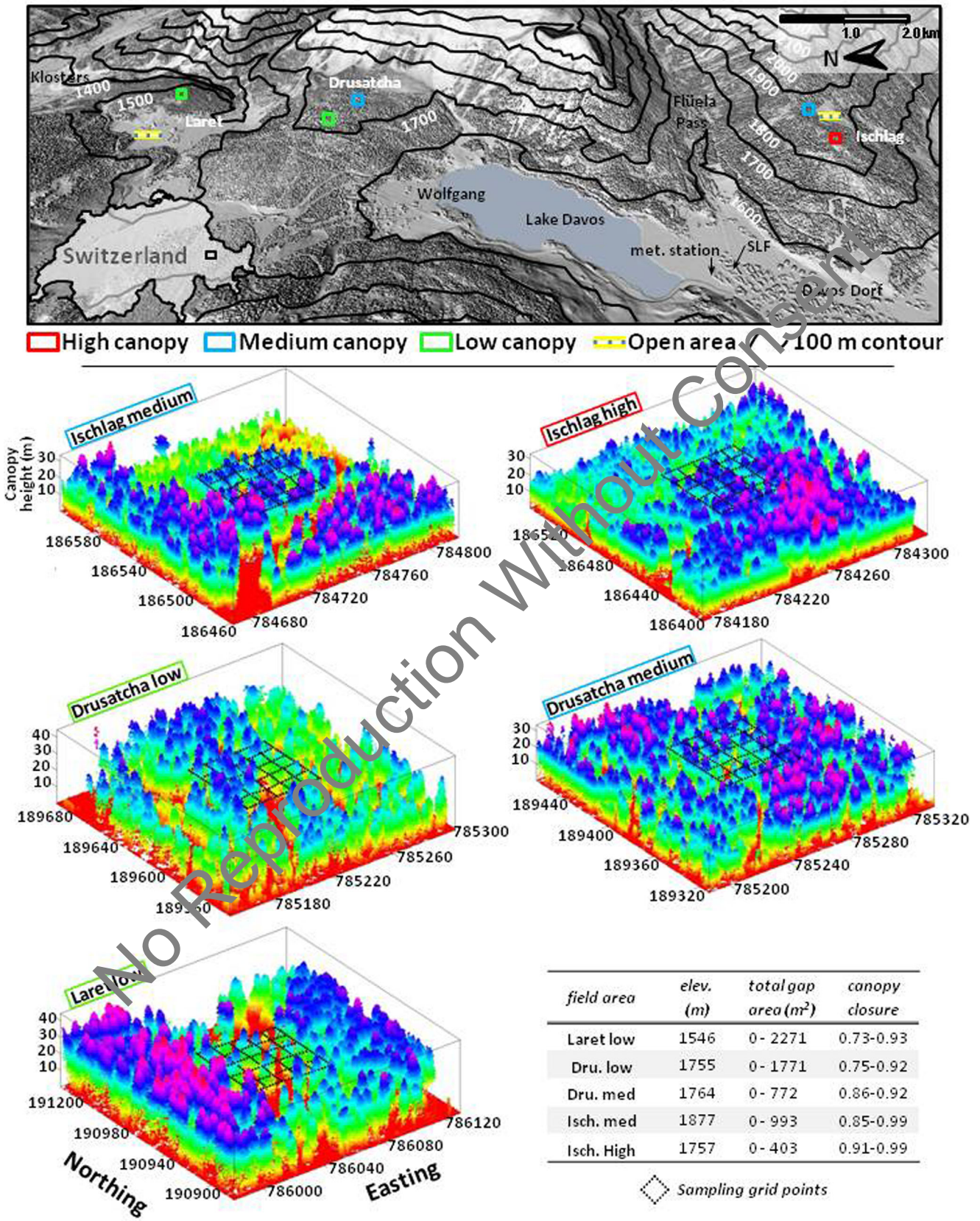

field area	elev. (m)	total gap area (m^2)	canopy closure
Laret low	1546	0 - 2271	0.73-0.93
Dru. low	1755	0 - 1771	0.75-0.92
Dru. med	1764	0 - 772	0.86-0.92
Isch. med	1877	0 - 993	0.85-0.99
Isch. High	1757	0 - 403	0.91-0.99

◇ Sampling grid points

Figure 1. Five forested field areas and two open areas are located at three elevation bands surrounding Davos. The box plots are LiDAR data cloud representations of the forested field areas. Each field area contains a measurement grid (50 m × 50m) with 276 surveyed and marked points. Each field area has unique forest gap fractions and highly heterogeneous canopy characteristics, as displayed in the bottom right corner.

$$\text{snow density} = 67.92 + 51.25\ e^{(T/2.59)} \quad (1)$$

Average air temperature (T) during each storm at each field site was derived from temperature lapse rates (individually derived for each storm event). These were based on an altitudinal gradient from four IMIS (Intercantonal measurement and information system) meteorological stations surrounding Davos, Switzerland, at 4 elevations bands: IMIS-KLO (Klosters) – 1560 m, IMIS-SLF (Davos) – 2140 m, IMIS-PAR (Parsenn) – 2290 m, IMIS-WFJ (Weissfluhjoch) – 2540 m. They yield an average RMSE of 0.38°C.

2.4. Canopy and Forest Metrics

Aerial LiDAR data were used to derive all canopy metrics: CC, LAI, total gap area (m^2), and mean distance to canopy (m). LiDAR acquisition was carried out in September 2010 from a helicopter flyover using the Riegl LMS Q 560 sensor. The average echo density was 36/m^2 with a shot density of 10/m^2 (density of last returns).

Canopy closure was derived using the method from *Moeser et al*. [2014] where the LiDAR data were used to create hemispheric-like images (synthetic images) at all surveyed points. The synthetic images were processed using the software "Hemisfer" [*Schleppi et al*., 2007; *Thimonier et al*., 2010], and LAI and CC were derived for each point. The LiDAR-based estimates of CC and LAI resulted in a correlation of 0.93 for CC and 0.83 for LAI when compared to estimates based on true hemispherical photography at 112 locations within the field areas [*Moeser et al*., 2014].

Total gap area (TGA) and mean distance to canopy (MDC) were derived using a vector searching algorithm developed by *Moeser et al*. [2015a]. It analyzes the dimensions of open areas as seen from a specific point in 192 unique directions (in a 2D projection) and calculates the open area based on this directional analysis (TGA). MDC was defined as the average distance of each of the 192 search directions (distance from the point to a canopy element). This process was run for each of the 1276 forest field points.

2.5. Meteorological Input Data

All meteorological input data were collected from the SwissMetNet (automatic meteorologi cal stations run by MeteoSwiss) station DAV2 (http://www.meteoschweiz.admin.ch/home.html?tab=overview). It is located <5 km from all field sites at 1594 m.a.s.l. (labeled as "met. station" in Figure 1). For ISWR, ILWR, Rh, V, and Ps the measured values were used for all field areas, whereas T_a, R_f and S_f were adjusted to better match the specific meteorological conditions of each field area, as explained below. All data were used at hourly time steps.

Temperature was interpolated to each field area by applying the commonly used atmospheric lapse rate (L_r) of −6.5 K per 1000 m of elevation gain:

$$T_{corr} = T_{metstation} + L_r(Alt._{fieldstation} - Alt._{metstation}) \quad (2)$$

where T_{corr} is the corrected temperature (at all time steps) for each site, which depends on the elevation difference (in meters) between the field stations ($Alt._{fieldstation}$) and the meteorological station ($Alt._{metstation}$).

The DAV2 station used a heated gauge to measure precipitation. Therefore a partitioning scheme was needed to separate solid (f_{solid}) from liquid precipitation (f_{liquid}). There is a considerable amount of work on solid versus liquid partitioning [*Kienzle*, 2008; *Marks et al*., 2013; *Rohrer*, 1989; *Ye et al*., 2013]. However, a modification of the S-shaped function proposed by *Kavetski and Kuczera* [2007] was implemented because it was locally calibrated. The threshold temperature, T_p (1.2°C), which denotes the temperature at which precipitation is 50% solid, and a further parameter, Mp (0.4), which controls the width of the function, were calibrated at the nearby Weissfluhjoch meteorological station from prior work by *Wever et al*. [2014]:

$$f_{liquid} = \frac{e^{\frac{T_a - T_P}{m_p}}}{1 + e^{\frac{T_a - T_P}{m_p}}} \quad (3)$$

$$f_{solid} = 1 - f_{liquid} \quad (4)$$

where f_{liquid} and f_{solid} are the relative fractions of liquid and solid precipitation, respectively.

The undercatch of solid precipitation from the heated gauge was corrected by a direct comparison of manual SWE measurements made at the station during the accumulation season from the past 35 years to the cumulative precipitation values from the gauge (as in *Egli et al*. [2009]). The data series was parsed to exclude time

periods with temperatures over 0°C. This gave a series of cold periods during accumulation. The difference between the first manual SWE measurement (SWE_{t0}) and last SWE measurement (SWE_{tend}) during each of the cold periods were calculated and divided by the total cumulated precipitation (P) from the gauge:

$$\text{undercatch} = \frac{(SWE_{t_{end}} - SWE_{t_0})}{\sum_{t_0}^{t_{end}} P_t} \quad (5)$$

All undercatch estimates were averaged, and this value (30% undercatch) was used as a multiplier to the precipitation data from the gauge.

A strong precipitation gradient is present across the Davos region. In general, the sites at Laret and Drusatscha receive more precipitation than the Ischlag sites and the meteorological station (Figure 1). Due to this, a comparison was made between measured SWE at the Laret open area and at the meteorological station. The same was done for the Ischlag open area. The equivalent methodology as the above undercatch analysis was utilized to account for the horizontal precipitation gradient per site and on a yearly basis.

2.6. New Interception Model

2.6.1. Description and Changes

Moeser et al. [2015b] defined I_{max} (mm SWE), i.e., the maximum amount of interception on a canopy element, as a function of the $\log_{10}$ of mean distance to canopy (x1), log of canopy closure (x2), and log of total gap area (x3):

$$I_{max} = 2.167(x1) - 3.410(x1)^2 + 55.761(x2) - 181.858(x2)^2 - 2.493(x3) + 0.499(x3)^2 + 20.819 \quad (6)$$

The I_{max} function was combined with a sigmoidal distribution of interception where I or interception (mm SWE) was defined as:

$$I = \frac{I_{max}}{1 + e^{-k(P - P_o)}} \quad (7)$$

where P is total storm precipitation, and the constants k and P_o are 0.3 and 13.3, respectively. However, this equation could not be directly implemented for time series data because storm precipitation cannot be used in a model framework that utilizes discrete model time steps. Therefore this equation was changed to represent dI/dt (i.e., the rate of change of snow held in the forest canopy) per equivalent time step unit.

However, two hurdles were encountered when converting equation (7) into a differential form. To ensure consistency with the law of mass conservation, dI/dt cannot exceed dP/dt, or equivalently dI/dP must be ≤ 1. However, while a rare occurrence, equation (7) can result in interception rates that exceed precipitation rates for certain values of I_{max} (Figure 2).

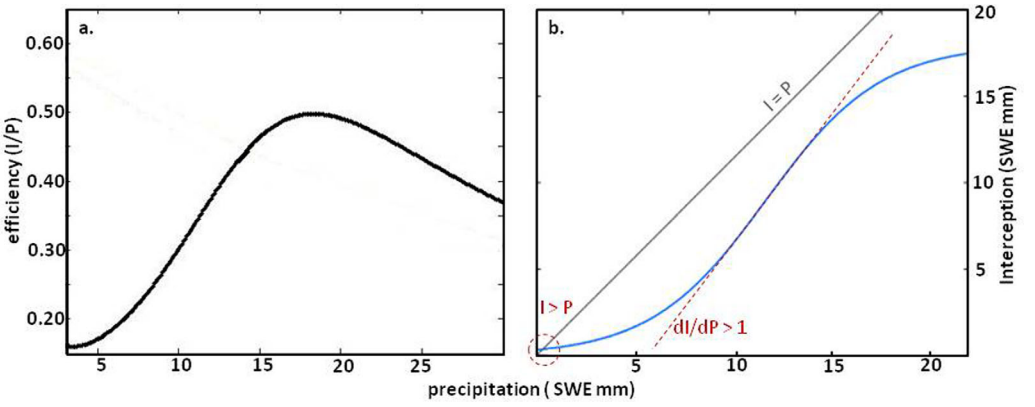

Figure 2. (a) Original efficiency curve as published in *Moeser et al.* [2015b]: snow bridging is represented by the efficiency increase to a maximum, at which point branch bending outcompetes bridging, thus leading to a decline in efficiency. (b) Interception curve (blue): the red circle shows that where precipitation values are small, this model version led to interception greater than precipitation. The red line shows where (dependent upon Imax), the derivative of the interception function can exceed unity.

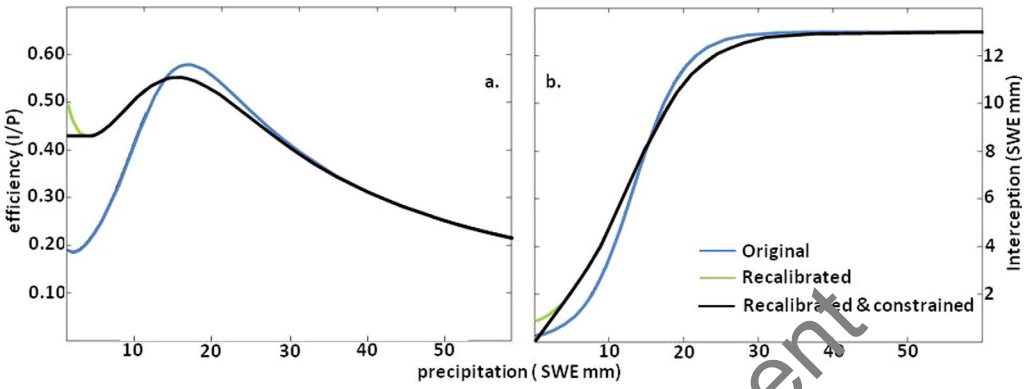

Figure 3. (a) Interception efficiency for Imax = 13.0 mm SWE. (b) Interception for Imax = 13.0 mm SWE. The blue lines represent the original Moeser et al. model (equation (7) with k = 0.3 and Po = 13.3). The green lines show the recalibrated model (k=0.215 and Po = 12.483). The black lines show the recalibrated and constrained model (from equations (11) and (12)).

If P is explicitly solved, then

$$P = -\frac{1}{k}\ln\left(\frac{I_{max}}{I} - 1\right) + P_0 \tag{8}$$

$$\frac{dI}{dP} = -\frac{kI}{I_{max}}\left(I_{max} - I\right) \tag{9}$$

Equation (9) must fulfill the condition of $dI/dP \leq 1$ in order to ensure no errors are introduced in the mass balance. Solving for I when the derivative of dI/dP is set to 0 and reinserting this term into equation (9) leads to the following constraint:

$$\frac{kI_{max}}{4} \leq 1 \tag{10}$$

When the initially proposed k of 0.3 and P_o of 13.3 were used, equation (10) was not fulfiled with $I_{max} > 13.3$ mm of SWE. Therefore k and P_o were re-optimized, but now with the constraint of equation (10). The optimization process followed the exact methodology used for the initial model development [*Moeser et al.*, 2015b], which was based upon the minimization of the RMSE of the actual versus model values (from equation (7)). This led to updated values of k = 0.215 and P_o = 12.483 (Figure 3).

The second hurdle was encountered when considering extremely low precipitation events, which were not present in the data used to develop the interception model, led to overestimations (albeit very small) of interception efficiency because $I > 0$ for P close to zero (equation 7, red circle in Figure 2b). This is a structural problem that cannot be circumvented when using this sigmoidal function. To account for this, the interception function was forced to pass through the origin by defining an interception threshold:

$$I_{thresh} = \frac{I_{max}}{1 + e^{-k(5-Po)}} \tag{11}$$

$$dI/dP = I_{thres}/5 \text{ mm}, \text{ if } I < I\_thres \tag{12}$$

2.6.2. Model Implementation

To incorporate equations (7), (11) and (12) into FSM, a new variable, P_{total} was introduced that cumulates precipitation and allowed for conversion between storm steps and uniform time steps. Thus, interception is calculated using the following set of equations.

$$I(t) = \frac{I_{max}}{1 + e^{-0.215[P_{total}(t) - 12.483]}} \tag{13}$$

$$I^*(t) = I(t) - \text{sublimation}(t) - \text{unloading}(t) \tag{14}$$

where I*(t) is interception at time t with sublimation and unloading removed, and

$$P_{total}(t) = P^*(t-1) + P(t) \quad (15)$$

when $I^*(t) \leq I_{thresh}$:

$$P^*(t) = \frac{I_{thresh}}{5} P(t) \quad (16)$$

when $I^*(t) > I_{thresh}$:

$$P^*(t) = \frac{1}{-0.215} \ln\left[\frac{I_{max}}{I^*(t)} - 1\right] + 12.483 \quad (17)$$

2.7. Standard Interception Model

The standard interception model from *Hedstrom and Pomeroy* [1998] defined I_{max} as a function of LAI:

$$I_{max} = 5.9\left(0.27 + \frac{46}{\rho_{snow}}\right) LAI \quad (18)$$

where ρ_{snow} (kg m^{-3}) is the density of falling snow and the multiplier of 5.9 is specific for spruce trees. I_{max} was combined with an exponential decay function of interception:

$$I = I_{max}\left(1 - e^{-\frac{P}{I_{max}}}\right) \quad (19)$$

where P is precipitation. The model was implemented into the FSM following the method of *Hedstrom and Pomeroy* [1998] and *Pomeroy et al.* [1998].

2.8. Canopy Snow Removal: Unloading and Sublimation

2.8.1. Unloading

Unloading is a complex process which is dependent upon precipitation characteristics (timing, duration, amount and density), wind (speed and direction), temperature, canopy characteristics, and branch flexibility. Due to these complexities, unloading represents a major research gap in forest snow hydrology to date [*Hedstrom and Pomeroy*, 1998; *Liston and Elder*, 2006; *Roesch*, 2006]. Since the primary goal of this work was to analyze the sensitivity of a new interception algorithm by gauging its performance against a standard model, the standard unloading model could not be used, as it unloads different amounts of intercepted snow on a canopy element in approximately the same amount of time. This eliminates any potential differences in snow on the ground from differing interception models. Due to this, we implemented (in both parameterizations of interception) a variant of the model introduced by *Liston and Elder* [2006] that was used in "SnowModel" [*Liston and Elder*, 2006] and "AMUNDSEN" [*Strasser et al.*, 2008b; *Strasser et al.*, 2004]:

$$\text{unloading} = 5.8^* 10^{-5}(T_a - 273.16) \quad (20)$$

where unloading (mm/second) is a direct function of air temperature (T_a in °K), gives an unloading rate of 5 mm/day per °K above 0°C and is only applied when temperature is above 0°C. We modified the stepwise function proposed by *Liston and Elder* [2006] to a continuous unloading function to allow for limited snow unloading snow even below 0°C (starting from −5°):

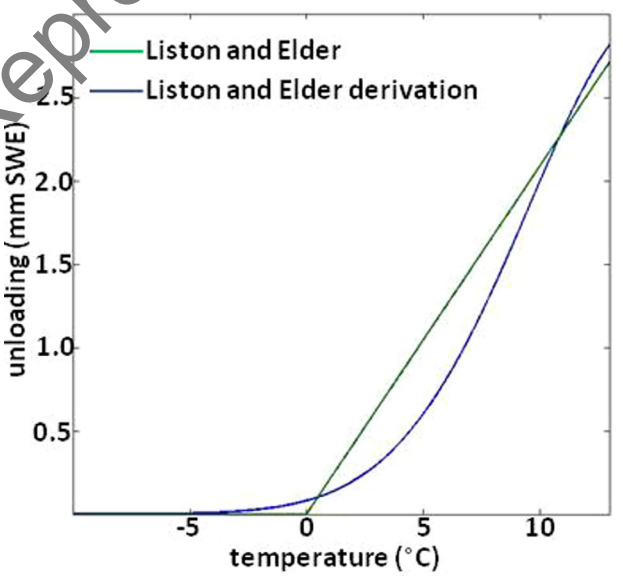

Figure 4. Comparison of the stepwise *Liston and Elder* [2006] model (green) and a continuous function (in blue).

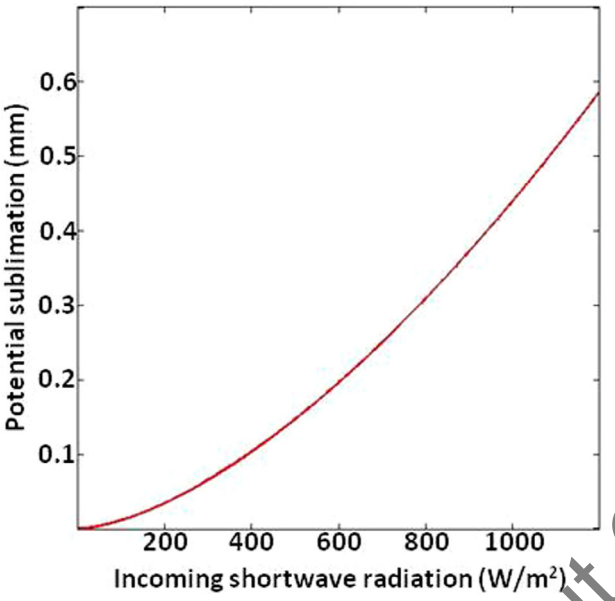

Figure 5. Potential sublimation as a function of ISWR.

$$\text{unloading} = 3.022 * e^{\frac{-(Ta-258.15)^2}{63.28}} \quad (21)$$

Like the original Liston et al. model, equation (21) does not capture many of the complexities found in the unloading process. However, unlike pure temporal decay functions such as the standard unloading model, it accounts for temperature effects on unloading and can be used for discrete time steps at all temperatures (Figure 4).

Note that the new interception model implemented in FSM was developed based on data collected after storms that inherently included snow that was unloaded during snowfall. Due to this, the unloading function was not applied during snowfall events.

2.8.2. Sublimation

Sublimation of snow in the forest canopy is traditionally modeled by calculating the energy balance of snow on the forest canopy [*Pomeroy et al.*, 1998]. However, in its current form, FSM does not have the capability to model the energy balance of snow on the canopy. Instead, a new sublimation model based on values typical for this area (calculated at a neighboring field site [Seehorn: 46.815, 9.856] from eddy covariance estimates) was developed. Minimum, mean and maximum sublimation values were evaluated, and a power function was fitted to incoming solar radiation data

$$potential\ \ sublimation = 3.54 * 10^{-4} ISWR^{1.070} \quad (22)$$

This power function reflects min/mean/max sublimation values, from the input of min/mean/max measured ISWR values from the meteorological station. Potential sublimation in mm/hour is the potential amount of sublimation that can occur during a time step Δt (Figure 5). Actual sublimation is dependent on the amount of snow remaining in the canopy (if any); if the amount of remaining canopy snow is less than or equal to the potential sublimation rate then all remaining snow is sublimated. This model (equation (22)) gave an

Table 1. Review of Average and Maximum Sublimation Rates as Well as the Fraction of Annual Snowfall Sublimated From Prior Studies

Mean Rate	Maximum Rate	% Sublimated	Location	Method	Study
0.2/hour	0.5/h	–	Scotland	mass balance	*Calder* [1991]
0.51/day	1.5/day	–	Colorado	weighing tree	*Schmidt* [1991]
–	0.7/h/3.3/day	–	Sweden	weighing tree	*Lunberg and Halldin* [1994]
–	4.0/36 h	–	Saskatchewan	–	*Harding* and *Pomeroy* [1996]
0.24/hour	0.56/h/3.9/7 h	–	Scotland	Gamma ray attenuation	*Lundberg et al.* [1998]
–	3/day	38–45%	Saskatchewan	weighing tree	*Pomeroy et al.* [1998]
0.6/day	2.3/day	–	Japan	eddy covariance	*Nakai et al.* [1999]
–	2.5/day	20–30%	global	model	*Essery et al.* [2003]
1.0/day	4.3/7 h	14%	SW Oregon	weighing tree	*Storck et al.* [2002]
0.70/day	3.7/day	–	Colorado	eddy covariance	*Molotch et al.*[2007]
1.31–1.64/day[a]	–	≤50%	Austrian Alps	model	*Strasser et al.* [2008a]
0.55/day	1.6/day	50%	N. America/Europe	model	*Ellis et al.* [2010]
–	–	32%	Colorado	mass balance	*Wilm and Dunford* [1945]
–	–	24%	East. Oregon	mass balance	*Miner and Trappe* [1974]
–	–	40%	–	–	*Meiman and Grant* [1974]
–	–	32–36%	Sasketchewan	mass balance	*Pomeroy and Gray* [1995]
–	–	32–45%	Sasketchewan	mass balance	*Pomeroy et al.* [1998]
–	–	39–45%	Yukon	mass balance	*Pomeroy et al.* [1999]
–	–	20–30%	–	–	*Montesis et al.* [2003]

[a]Assuming 5 months of S_f precipitation.

average value of 0.35 mm/day and a maximum of 3.48 mm/day of potential sublimation (from this data set). While this is a simplified approach, it produced reasonable values of sublimation that were comparable with prior studies (Table 1).

2.9. FSM Model Application

The FSM model was run at 1276 points for the 2012 and 2013 field seasons. The FSM configurations for each of the interception models (standard model and *Moeser et al.*) were grouped at each time step and the median value at each step was taken. This gave median values (as well as a range) for each output parameter from the FSM (SD, SWE, etc) for each interception parameterization at each time step. The median values from each interception model were compared. Specifically, the sensitivity between the interception parameterizations was analyzed for the effect on (1) interception estimation, and (2) under-canopy SWE and under-canopy SD. These differences were primarily assessed using a comparison to the distribution of the forest canopy, in order to better estimate how well the forested environment has been represented and whether the heterogeneity of the forested environment has been captured down the modeling chain.

3. Results and Discussion

The initial interception model was successfully integrated into the FSM model at hourly time steps from the integration of equations 11 – 17. This new system of equations demonstrated a similar fit to interception events as the original storm-based model.

The *Moeser et al.* [2015b] model reproduced storm interception events with an R^2 of 0.65 and RMSE of 3.39 mm. When k and P_o were re-optimized using the constraint from equation (10), no change was seen in R^2, and the RMSE remained virtually the same (3.40). The standard model [*Hedstrom and Pomeroy*, 1998] had an R^2 of 0.39 and RMSE of 5.19 mm. Below we have analyzed how these model differences transferred into contrasts in under-canopy snow and demonstrated how these contrasts relate to forest canopy characteristics.

The field points show a large spatial variation of canopy parameters, with total gap area ranging from 0 to 2250 m^2, mean distance to canopy ranging from 0 to 23.7 m and LAI ranging from 1.2 to 8.0. Logically, these large variations should be seen in the results, with low interception at points with a high openness (high TGA and MDC) and high interception in areas with low openness (low TGA and MDC), with the closed canopy areas having even higher interception with progressively higher LAI or CC values. Furthermore, the trends in interception estimations as they relate to the canopy should also be seen in the under-canopy SWE and SD estimates.

3.1. Interception and Under-Canopy Snow

Despite the fact that some simulated points showed similar under-canopy SWE estimations between the two interception modules (Figure 6, top), the majority of the points featured large deviations (Figure 6, bottom). The under-canopy SWE estimates using the *Moeser et al.* model were generally improved, due to the inclusion of new metrics of forest structure (i.e., TGA, MDC). Specifically, the largest differences between the two models were found at the canopy–open area interface and at open areas which were described by TGA and MDC.

To demonstrate this, two points with similar canopy closure (0.90 versus 0.92) but different TGA (68.81 m^2 versus 541.62 m^2) and MDC (2.01 m versus 10.75 m) that are located approximately 8 m apart were analyzed (Figure 7, for locations of the points see Figure 8). The use of the standard interception model yielded almost equivalent cumulative interception and sublimation estimates (and therefore also SWE and snowmelt), while use of the *Moeser et al.* model simulated substantial differences.

TGA and MDC had further effects on the behavior of the two FSM groupings (i.e., the Moeser et al. interception grouping and the standard interception grouping) on larger scales. Figure 8 displays the cumulative interception for all points within the Drusatcha Medium field area along with the overlying canopy structure. The open areas and canopy-open area interfaces can be visualized (Figure 8, left), and when these features are compared to the simulation output, significant differences between the modeling approaches become evident. Furthermore it displays (as with the point-based analysis in Figure 7) nearly equivalent

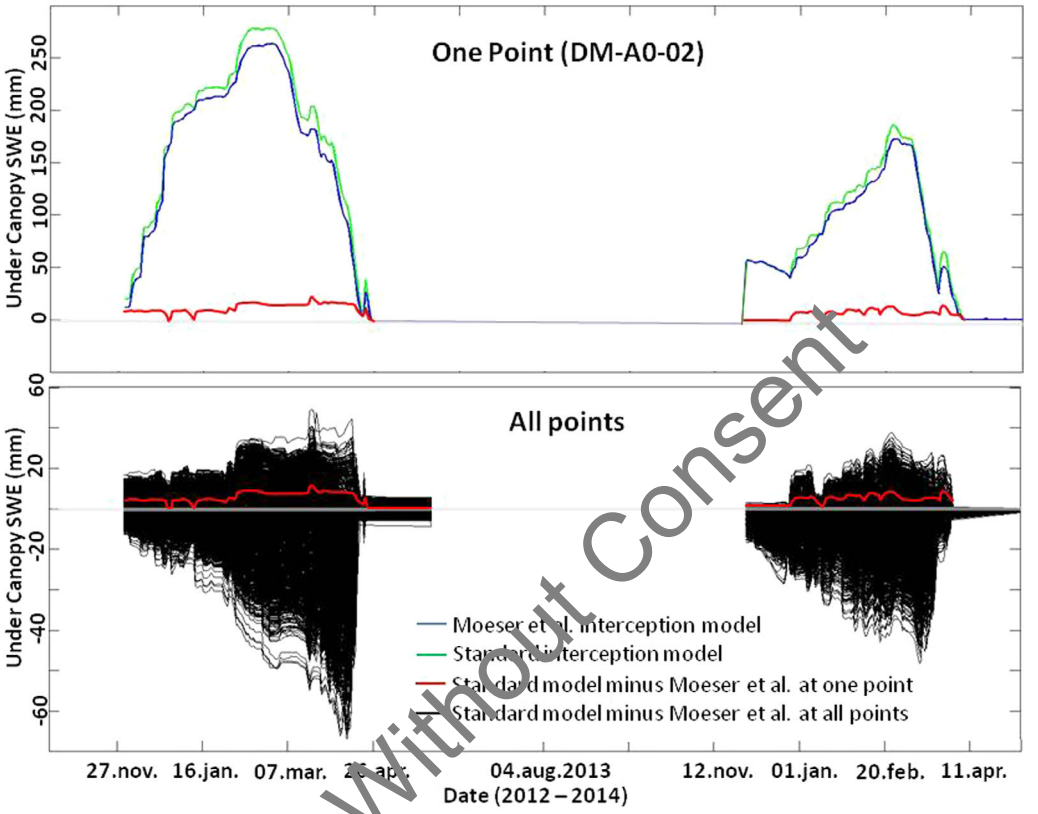

Figure 6. (top) Comparison of under-canopy SWE at point A0-02 in the Drusatcha Medium (DM) field area when using the standard interception model (green) versus the Moeser et al. interception model (blue) and their difference (red). While some field points feature similar under-canopy SWE estimates, such as this point, many points show substantial differences between the two interception modules. (bottom) Difference of under-canopy SWE from the two interception models at all points (black), with the red difference line from point A0-02 (top) being displayed again in the bottom plot.

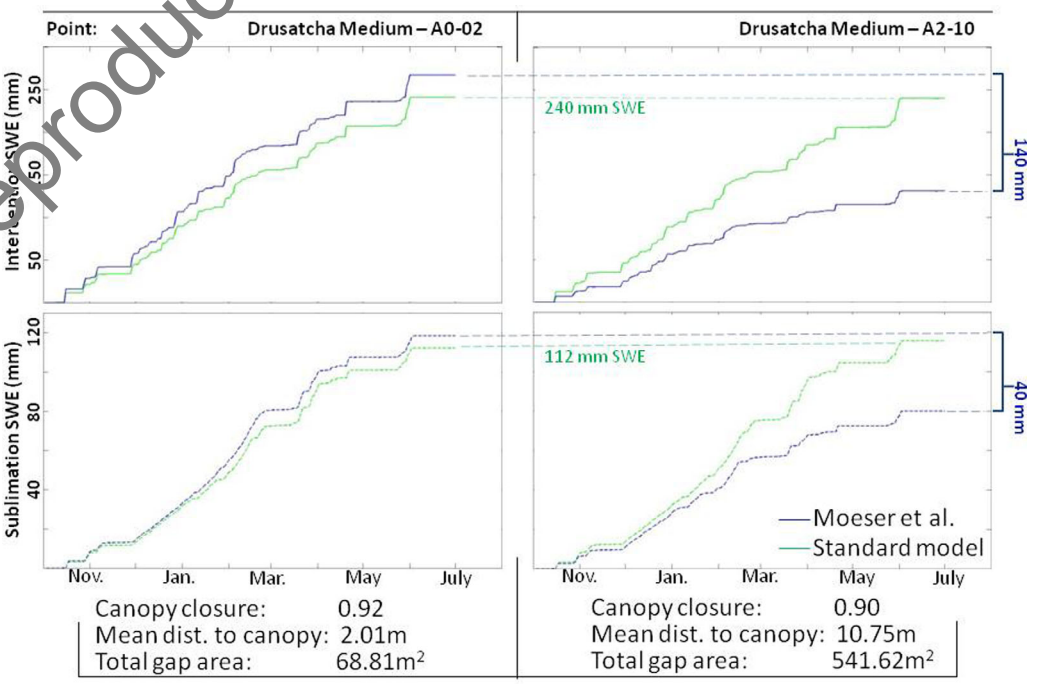

Figure 7. The point on the left (A0-02) and the point on the right (A2-10) have similar CC values (0.90–0.92) but display very different forest scale metrics. (top) cumulative interception for the 2012/2013 winter season. (bottom) cumulative sublimation for the 2012/2013 winter season. Locations of these points can be seen within Figure 8.

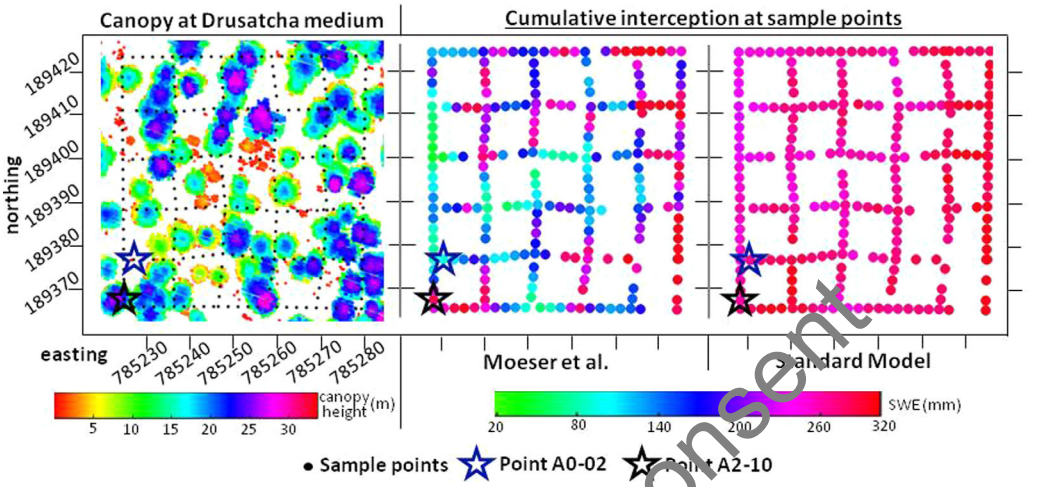

Figure 8. (left) Canopy height at the field area Drusatcha Medium. (middle) Cumulative interception estimates from the Moeser et al. model. (right) Cumulative interception estimates from the standard model. The points from Figures 6 and 7 are labeled as stars.

cumulative interception estimates at all points within the field area when the standard interception model was applied (Figure 8, right). This is contrasted to the *Moeser et al*. model which displayed a significant cumulative interception estimation variance which closely mimicked the horizontal forest structure. At all points, the *Moeser et al*. cumulative interception estimates ranged from 25 to 310 mm SWE, whereas the estimates from the standard model ranged from 165 to 310 mm SWE.

Similar patterns were evident from the simulated under-canopy SD for the peak of the winter 2012/2013 (Figure 9): the *Moeser et al*. model displayed much greater variation in estimated values, ranging from 55 cm to 83 cm on the ground compared with 53 cm to 67 cm from the standard model.

Although both models showed some degree of absolute biases (of ~20 cm SD which can be seen in the disparate scale bars in figure 9), the *Moeser et al*. model output was more consistent with ground observations compared to the standard model. Absolute SD estimates from the *Moeser et al*. model were reasonably close to observations and the spatial pattern was very similar. This was not the case for the standard model, where some of the low simulated values (blue colors) were associated with high observed values (red

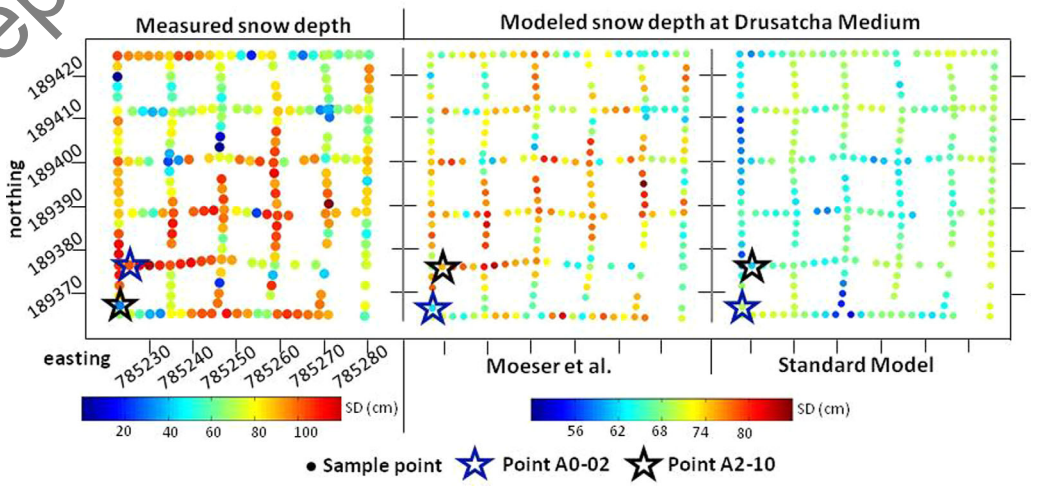

Figure 9. (left) Measured snow depth at the peak of winter 2012/2013. Center: Simulated SD when using the Moeser et al. interception model. (right) Simulated SD when using the standard interception model. Similar to the interception estimates (Figure 7), the standard model showed fairly homogenous estimates throughout the field area, while simulated SD from the Moeser et al. model features heterogeneous values and displayed a similar pattern as in the measured data.

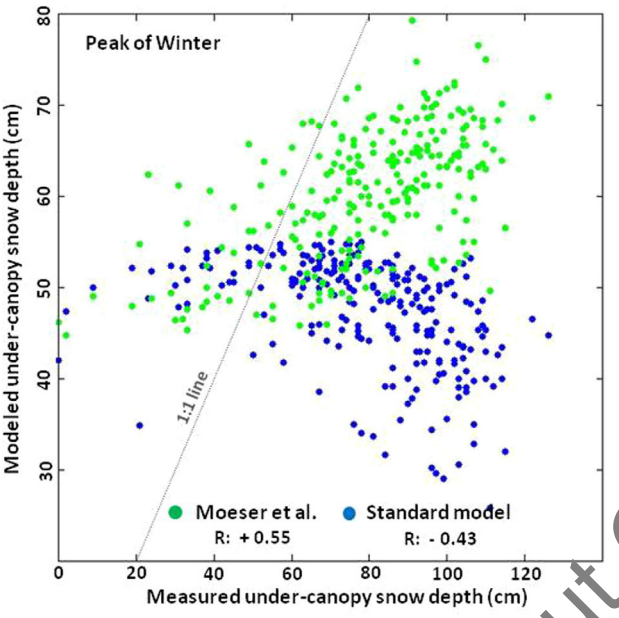

Figure 10. Comparison of simulated and measured under-canopy snow depth in the Drusatscha Medium field area. The negative correlation in the standard model is primarily due to interception overestimates in open areas. The RMSE of the Moeser et al. and the standard model are 23 and 29 cm of snow depth, respectively.

colors; cf. Figure 10). This inverse correlation present within the standard model can be visualized within a plot of observed versus modeled snow depth in figure 10. See section 3.4 for further analysis.

3.2. Unloading and Sublimation

The larger range in estimation variance from the *Moeser et al.* interception model was also evident in simulated unloading and sublimation estimates. Sublimation ranged from a maximum of 0.79 to 3.48 mm/day SWE (depending on I_{max}), with a mean of 0.05 to 0.47 mm/day SWE, which amounted to 2.6 to 31% of total winter precipitation (or 3 to 42% of total winter snowfall). This was more than double the variance compared to the standard interception model (Figures (11 and 12)). Although these numbers would vary if other unloading and sublimation models were used, the magnitude of the estimation variance between the two interception models would remain similar since they are a function of the amount of intercepted snow on the canopy. Furthermore, these results were comparable to those of prior studies (Table 1).

3.3. Precipitation Event Size

The differences in the output of the two interception models were not only related to canopy structure variables. Structural differences between the models also resulted in varying responses to the size of precipitation events. Frequent small storms, which characterize the study areas, led to higher estimations of interception from the standard model compared to the estimations from the *Moeser et al.* model, whereas large storms, which are atypical of the area, led to lower estimations from the standard model. This was also evident from the storm event analysis [*Moeser et al.*, 2015b, Figure 6] where interception was underestimated by the standard model for large storms and overestimated for small storms. This was due to the function describing interception efficiency (Figure 13), which in the standard model was modeled as an exponential decay. This allowed for large amounts of freshly fallen snow to be intercepted early in a storm event. In contrast, the Moeser et al. interception model started with a lower interception efficiency, which increased as the storm continued due to snow

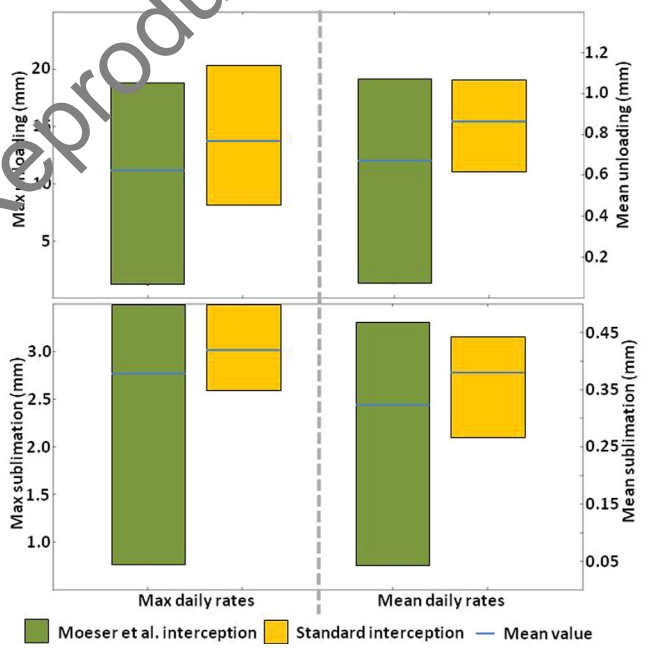

Figure 11. (left) Maximum simulated daily unloading and sublimation rates according to both models. (right) Simulated mean daily rates at all points. The range of values represents the variability between sample points.

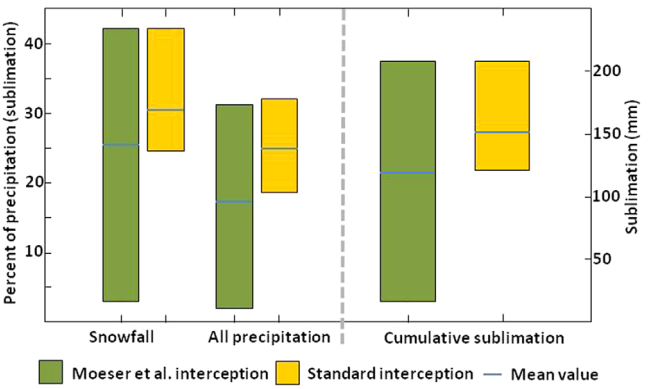

Figure 12. (left) Percent of total precipitation that was sublimated according to both models. (right) Cumulative sublimation values for the 2012/2013 season at all points.

bridging and then decreased due to branch bending. While, for large precipitation events, both models may reach a maximum interception, the underlying efficiency has systematic consequences on the mass balance if a snow storm does not reach this point.

The effect of the precipitation distribution was visualized from an analysis of P_{total}, which is a proxy for cumulative storm precipitation (Figure 14). When P_{total} was <5 mm, the Moeser et al. model showed significantly higher hourly interception values than the standard model. When P_{total} was <5 mm, the standard model displayed higher hourly interception estimations in areas with moderate to high MDC and TGA values. Thus, if the standard model is to be utilized in forests that are characterized by snow bridging and large storm events prevail, the interception would be underestimated and under-canopy snow over-estimated. The opposite applies to areas characterized by frequent small precipitation events (such as Davos).

3.4. Sensitivity Analysis

The FSM model used basic parameterizations of various processes [*Essery*, 2015], including the unloading and sublimation routines proposed in this paper. These simplifications can be seen in the difference between the goodness-of-fit statistics between interception estimates and the under-canopy snow depth estimates (Table 2, Figure 15). The correlation coefficient of under-canopy SD (for both interception models) was approximately 20% lower compared to the correlation coefficient of interception estimates. Still, the sensitivity behind using two disparate interception models could be analyzed relative to the forest structure. As the size of forest gaps increased (openness), the standard model lost the ability to estimate interception and under-canopy snow. The new model, however, showed no major degradation in the correlation coefficient as forest stand openness increased for the interception and under-canopy snow estimates (Figure 15). This was due to the inclusion of forest metrics that were able to resolve where a point was located relative to an open area (i.e., open areas have low to no interception). This was contrasted by the point-based metrics in the standard model that were unable to determine where an open area begins and ends (LAI, CC).

3.5. Transferability and Research Gaps

Despite of the key steps forward that are represented by the new snow interception model developed here, this project has highlighted the complexity of modeling under-canopy snow as well as several important research gaps.

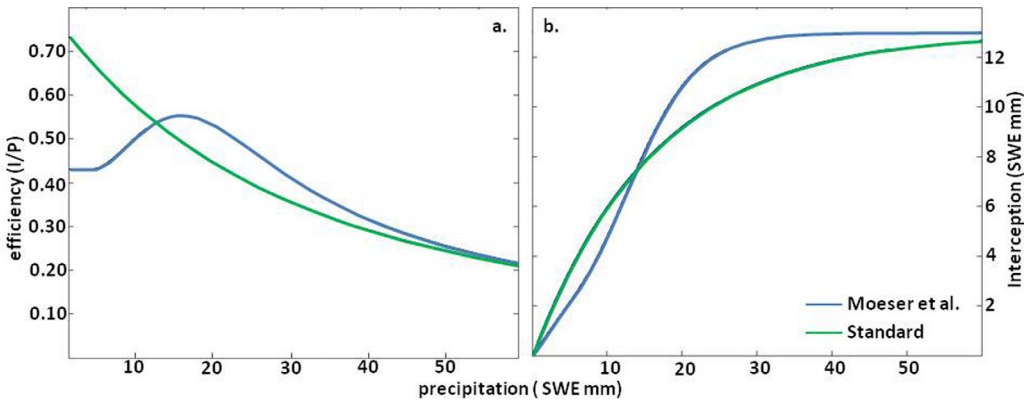

Figure 13. (a) efficiency curves from the two interception models for Imax = 13.0 mm SWE. SWE. (b) Interception curves Imax = 13.0 mm SWE.

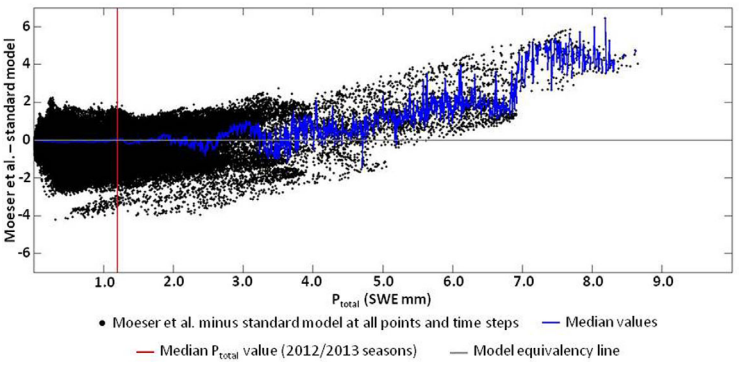

Figure 14. Analysis of the effect of precipitation distribution on simulated interception. P total is a proxy for total storm precipitation and was calculated every hour for the 2012 and 2013 season. At large storm events, the Moeser et al. model gives higher estimates than the standard model, whereas for small storms, the standard model gives higher values when the simulated areas have medium to high TGA and MDC values.

Due to the indirect measurement technique for interception, no field measurements of unloading, melt and drip or sublimation were taken. Snow unloading is an extremely complex process that depends on the timing, duration, amount and density of precipitation (current and prior) falling onto the canopy (cf. section 2.8.1). Canopy and branch-bending characteristics in conjunction with precipitation further determine how much and where the snow will unload. Finally, temperature, wind and solar radiation dictate when the snow will unload. It is also common for snow to follow preferential unloading paths, e.g., when the unloaded snow falls from one particular side or section of the canopy. Research in warmer winter climates (e.g., Pacific Northwest, USA), beginning with work in Japan [*Shidei et al*., 1952] has also illustrated the importance of melt and drip processes (not modeled within FSM) and demonstrated its relationship to temperature [*Clark et al*. 2015b; *Friesen et al*., 2015; *Lundquist et al*., 2013; *Martin et al*., 2013]. However, quantifying the effects of intercepted snow on under-canopy SWE and runoff will not be fully possible until it is known how much and when intercepted snow falls to the ground in all climates.

It is unclear how this model (equations 1–17) would perform for forest types other than Norway spruce. In principle, the benefits of the new I_{max} model that utilizes stand-scale metrics should be species-independent. Yet, it is unclear how the variables k and P_o, which dictate the rate of interception efficiency and the maximum efficiency, may change if the model was transferred to new areas. It is possible that the formulation underlying these variables is related to snow density and/or tree species (as long as the constraint of equation (10) is not violated). Intuitively, this makes sense: the denser or "stickier" the snow, the higher the potential rate of snow bridging (up to a certain point at least).

Both interception models require detailed data to characterize the canopy. In both models, this is the primary flux in implementation over large model domains. LAI and CC (CC is utilized in both models and LAI is utilized in the standard model), require sufficiently high resolution remotely sensed data for effective derivation of these elements. Total gap area and mean distance to canopy (utilized only in the new model) have, to date, only been derived using high resolution LiDAR data. However, the estimation of these metrics does not require a high point cloud density. Furthermore, the algorithm that was used to derive these metrics first transformed the data into a grid, removing any dependence on a high point cloud density. TGA and MDC could potentially be derived from other, lower resolution gridded data sets. It is conceivable that

Table 2. Comparison of the Use of the Interception Models for Under-Canopy Snow Depth at Peak of Winter (4 April 2013) and Interception[a]

	Interception (mm- SWE)				Peak of Winter Snow Depth (cm)						
	r		*RMSE*		*r*		*RMSE*				
"Openness" Quantile	Moeser et al	Standard model	Moeser et al.	Standard model	Moeser et al	Standard model	Moeser et al.	*Standard model*	Total Gap Area (m^2)	Mean Dist. to Canopy (m)	Canopy Closure
≤ 25%	0.78	0.62	2.7	6.8	0.57	0.37	21	22	<27	<2	0.82–0.99
25–50%	0.67	0.45	3.5	5.6	0.48	0.26	18	20	27–181	2–6	0.81–0.99
50–75%	0.61	0.07	3.4	4.5	0.37	− 0.08	23	32	181–665	6–12	0.79–0.99
> 75%	0.52	−0.22	3.5	4.1	0.17	− 0.13	24	39	>665	>12	.70–0.99

[a]All points were grouped into quartiles based upon mean distance to canopy and total gap area to represent openness. For a visual analysis see Figure 15.

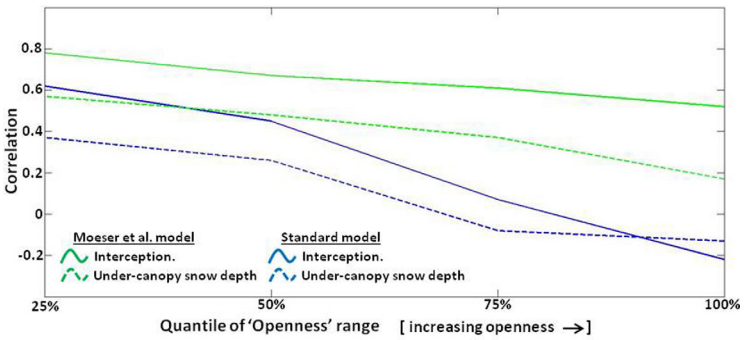

Figure 15. All points were grouped into quartiles based upon mean distance to canopy and total gap area to represent openness (x axis). The solid lines represent the correlation of interception estimates and the dotted lines represent under-canopy snow depth estimates. Note that the standard model (in blue) demonstrates reduced correlations as compared to the Moeser et al. and the initial correlations quickly diminish as openness of the field points increases (increase in TGA and MDC) which is not as apparent in the Moeser et al. model.

photogrammetric methods could be used in place of aerial LiDAR data to accurately derive these metrics (TGA, and MDC). It is also possible high resolution aerial imagery could be used, provided that information on the photo angle is retained.

4. Conclusion

The conversion of a storm based interception model to a model applicable at discrete model time steps was successfully achieved by the derivation of a new system of equations (equations (1–17)), which allowed for a numerically stable implementation in a large-scale snowmelt model, FSM. Given that the new interception model inherently includes unloading during snowfall, these guiding equations can be used in other snowmelt models as long as the corresponding unloading model is not utilized during snowfall events.

The inclusion of forest scale metrics (total gap area, and mean distance to canopy) in the *Moeser et al.* interception model had major impacts on simulated interception. The largest differences between the standard and the new interception model were evident at the canopy-open area interfaces and the open areas. The standard model showed very little variation of interception estimates regardless of differences in total gap area or mean distance to canopy, with a maximum cumulative seasonal interception range of ~145 mm SWE between all points. This was contrasted by the new interception model, which showed a variance of ~285 mm SWE between all points and a better fit with measured data. The variance within the new interception model was dictated by the canopy structure, with high interception values in dense canopy with low MDC and TGA values and subsequently lower interception estimates as MDC and TGA increased. Field points that feature similar CC can have very different large-scale canopy structures (MDA, TGA). However, the standard model is not able to discriminate between such points.

The spatial heterogeneity of the forest environment was also represented farther down the modeling chain in the new approach. Larger variations of under-canopy SWE/SD as well as sublimation were featured by the new model as compared to the standard model. The new interception module resulted in SD simulations that were consistent with the small-scale patterns evident from the ground observations. The updated FSM represents one of the first snowmelt models that is able to reflect the spatial variability in forest snow caused by local heterogeneity in the canopy.

The new function used to model interception efficiency had a systematic impact on interception estimates. It accounted for snow bridging and branch bending, where interception efficiency rose to a maximum with increasing precipitation and then decreased. This was contrasted by the standard model, which featured an exponential reduction of interception efficiency as precipitation increased. These differences demonstrated, at least for these study areas, which are characterized by frequent small storms, higher estimates of interception from the standard model in areas with moderate to large open areas. The opposite was also true, with large storms, the standard model led to lower estimates in all openness regimes. If the *Moeser et al.* interception model was implemented for climates characterized by large storms events, it would yield significantly higher interception estimations than the standard model (and subsequently lower under-canopy snow estimates).

While the benefits of the inclusion of new canopy structure parameters (MDC, TGA) should be universal, it remains to be seen whether a sigmoidal interception function is also suitable for other climates or other tree species. Further research should address the applicability of this interception model in different forest regions worldwide.

Acknowledgments
This project was funded by the Swiss National Science Foundation (SNF, project no. 200021_146184/1). Substantial field support was provided by Clare Webster, Nena Griessinger, Saskia Gindraux, Franziska Zieger, Franziska Zahner, Jiri Roubinek, and Mathias Rieckh from the Snow Hydrology Group of the WSL Institute for Snow and Avalanche Research SLF. Programming support was given by Dr. Jan Magnusson, also of the Snow Hydrology Group. Access to FSM and support was given by Richard Essery from the University of Edinburgh School of Geosciences. Detailed manuscript input was given by Harald Bugmann of the Forest Ecology from ETH, Zürich. All data used in this study are available upon request from the corresponding author (moeser@slf.ch).

References

Andreadis, K. M., P. Storck, and D. P. Lettenmaier (2009), Modeling snow accumulation and ablation processes in forested environments, *Water Resour. Res.*, *45*, W05429, doi:10.1029/2008WR007042.
Best, M. J., et al. (2011), The joint UK land environment simulator (JULES), model description–Part 1: Energy and water fluxes, *Geosci. Model Dev.*, *4*(3), 677–699.
Boone, A. (2009), *Description du Schema de Neige ISBA-ES (Explicit Snow)*, Cent. Natl. de Rech. Météorologiques, Mètèo-France, Toulouse, France.
Bründl, M., P. Bartelt, M. Schneebeli, and H. Flühler (1999), Measuring branch defection of spruce branches caused by intercepted snow load, *Hydrol. Processes*, *13*(14–15), 2357–2369.
Bunnell, F. L., R. S. McNay, and C. C. Shank (1985), Trees and snow: The deposition of snow on the ground—A review and quantitative synthesis, *IWIFR-17*, Res. Minist. of Environ. and Forests, Victoria, Canada.
Calder, I. R. (1991), *Evaporation in the Uplands*, John Wiley, Chichester, U. K.
Clark, M. P., et al. (2015a), A unified approach for process-based hydrologic modeling: 1. Modeling concept, *Water Resour. Res.*, *51*, 2498–2514, doi:10.1002/2015WR017198.
Clark, M. P., et al. (2015b), A unified approach for process-based hydrologic modeling: 2. Model implementation and case studies, *Water Resour. Res.*, *51*, 2515–2542, doi:10.1002/2015WR017200.
Clark, M. P., et al. (2015c), The structure for unifying multiple modeling alternatives (SUMMA), version 1.0: Technical description, *NCAR Tech. Notes NCAR/TN 514+STR*, Natl. Cent. for Atmos. Res., Boulder, Colo.
Cox, P.M., R. A. Betts, C. B. Bunton, R. L. H. Essery, P. R. Rowntree, and J. Smith (1999), The impact of new land surface physics on the GCM simulation of climate and climate sensitivity, *Clim. Dyn.*, *15*(3), 183–203.
Douville, H., J. Royer, and J. Mahfouf (1995), A new snow parameterization for the Meteo-France climate model part I: Validation in stand-alone experiments, *Clim. Dyn.*, *12*, 21–35.
Dutra, E., G. Balsamo, P. Viterbo, P. M. A. Miranda, A. Beljaars, C. Schär, and K. Elder (2010), An improved snow scheme for the ECMWF land surface model: Description and offline validation, *J. Hydrometeorol.*, *11*(4), 899–916.
Egli, L., T. Jonas, and R. Meister (2009), Comparison of different automatic methods for estimating snow water equivalent, *Cold Reg. Sci. Technol.*, *57*(2–3), 107–115.
Ellis, C. R., J. W. Pomeroy, T. Brown, and J. MacDonald (2010), Simulation of snow accumulation and melt in needle-leaf forest environments, *Hydrol. Earth Syst. Sci.*, *14*(6), 925–940.
Essery, R. (2015), A Factorial Snowpack Model (FSM 1.0), *Geosci. Model Dev. Discuss.*, *8*, 6583–6609.
Essery, R., and J. Pomeroy (2001), *Soil-Vegetation-Atmosphere Transfer Schemes and Large-Scale Hydrological Models*, pp. 343–347, Int. Assoc. of Hydrol. Sci., Maastricht, Netherlands.
Essery, R., J. Pomeroy, J. Parviainen, and P. Storck (2003), Sublimation of snow from coniferous forests in a climate model, *J. Clim.*, *16*(11), 1855–1864.
Esssery, R., N. Rutter, J. Pomeroy, R. Baxter, M. Stähli, M., D. Gustafsson, A. Barr, P. Bartlett, K. Elder (2009), SNOWMIP2 An evaluation of forest snow process simulations, *Bull. Am. Meteorol. Soc.*, 1120–1135.
Essery, R., S. Morin, Y. Lejeune, B. C. Ménard (2013), A comparison of 1701 snow models using observations from an alpine site, *Adv. Water Resour.*, *55*, 131–148.
Friesen, J., J. Lundquist, and J. T. Van Stan (2015), Evolution of forest precipitation water storage measurement methods, *Hydrol. Processes*, *29*, 2504–2520.
Golding, D. L., and R. H. Swanson (1986), Snow distribution in clearings and adjacent forest, *Water Resour. Res.*, *22*(13), 1931–1940.
Guntner, A., S. Stuck, P. Werth, P. Doll, K. Verzano, and B. Merz (2007), A global analysis of temporal and spatial variations in continental water storage, *Water Resour. Res.*, *43*, W05416, doi:10.1029/2006WR005247.
Harding, R. J., and J. W. Pomeroy (1996), Energy balance of the winter boreal landscape, *J. Clim.*, *9*(11), 2778–2787.
Hedstrom, N. R., and J. W. Pomeroy (1998), Measurements and modelling of snow interception in the boreal forest, *Hydrol. Processes*, *12*(10–11), 1611–1625.
Kavetski, D., and G. Kuczera (2007), Model smoothing strategies to remove microscale discontinuities and spurious secondary optima in objective functions in hydrological calibration, *Water Resour. Res.*, *43*, W03411, doi:10.1029/2006WR005195.
Kienzle, S. W. (2008), A new temperature based method to separate rain and snow, *Hydrol. Processes*, *22*, 5067–5085.
Kobayashi, D. (1987), Snow accumulation on a narrow board, *Cold Reg. Sci. Technol.*, *13*, 239–245.
Liston, G. E., and K. Elder (2006), A distributed snow-evolution modeling system (SnowModel), *J. Hydrometeorol.*, *7*(6), 1259–1276.
Lopez-Moreno, J. I., and J. Latron (2008), Influence of canopy density on snow distribution in a temperate mountain range, *Hydrol. Processes*, *22*(1), 117–126.
Lopez-Moreno, J. I., and M. Stähli (2008), Statistical analysis of the snow cover variability in a subalpine watershed: Assessing the role of topography and forest, interactions, *J. Hydrol.*, *348*(3–4), 379–394.
Lundberg, A., and S. Halldin (1994), Evaporation of intercepted snow: Analysis of governing factors, *Water Resour. Res.*, *30*(9): 2587–2598.
Lundberg, A., and S. Halldin (2001), Snow interception evaporation—Rates, processes and measurement techniques, *Theor. Appl. Climatol.*, *70*, 117–133.
Lundberg, A., I. Calder, and R. Harding (1998), Evaporation of intercepted snow: Measurement and modeling, *J. Hydrol.*, *206*(3–4), 151–163.
Lundquist, J. D., S. E. Dickerson-Lange, J. A. Lutz, and N. C. Cristea (2013), Lower forest density enhances snow retention in regions with warmer winters: A global framework developed from plot-scale observations and modeling, *Water Resour. Res.*, *49*, 6356–6370, doi: 10.1002/wrcr.20504.
Magnusson, J., N. Wever, R. Essery, N. Helbig, A. Winstral, and T. Jonas (2015), Evaluating snow models with varying process representations for hydrological applications, *Water Resour. Res.*, *51*, 2707–2723, doi:10.1002/2014WR016498.
Mahat, V., and D. G. Tarboton (2014), Representation of canopy snow interception, unloading and melt in a parsimonious snowmelt model, *Hydrol. Processes*, *28*, 6320–6336.
Marks, D., A. Winstral, M. Reba, J. Pomeroy, and M. Kumar (2013), An evaluation of methods for determining during-storm precipitation phase and the rain/snow transition elevation at the surface in a mountain basin, *Adv. Water Resour.*, *55*, 98–110.
Martin, K. A., J. T. Van Stan, S. E. Dickerson-Lange, J. A. Lutz, J. W. Berman, R. Gersonde, and J. D. Lundquist (2013), Development and testing of a snow interceptometer to quantify canopy water storage and interception processes in the rain/snow transition zone of the North Cascades, Washington, USA, *Water Resour. Res.*, *49*, 3243–3256, doi:10.1002/wrcr.20271.

Meiman, J. R., and L. Grant (1974), *Snow-Air Interactions and Management on Mountain Watershed Snowpack*, Colo. State Univ., Environ. Res. Cent. Bull., Fort Colins.
Miner, N. H., and J. M. Trappe (1957), Snow interception, accumulation and melt in lodgepole pine forest in the Blue Mountains of Eastern Oregon, United States Department of Agriculture Forest and Range Experimental Station Research Note no. 143.
Moeser, D., J. Roubinek, P. Schleppi, F. Morsdorf, and T. Jonas (2014), Canopy closure, LAI and radiation transfer from airborne LiDAR synthetic images, *Agric. For. Meteorol.*, *197*, 158–168.
Moeser, D., F. Morsdorf, and T. Jonas (2015a), Novel forest structure metrics from airborne LiDAR data for improved snow interception estimation, *Agric. For. Meteorol.*, *208*, 40–49.
Moeser, D., M. Stähli, and T. Jonas (2015b), Improved snow interception modeling using canopy parameters derived from airborne LIDAR data, *Water Resour. Res.*, *51*, 5041–5059, doi:10.1002/2014WR016724.
Molotch, N. P., P. D. Blanken, M. W. Williams, A. A. Turnipseed, R. K. Monson, and S. A. Margulis (2007), Estimating sublimation of intercepted and sub-canopy snow using eddy covariance systems, *Hydrol. Processes*, *21*(12), 1567–1575.
Montesi, J., K. Elder, R. A. Schmidt, and R. E. Davis (2003), Sublimation of intercepted snow within a subalpine forest canopy at two elevations, *J. Hydrometeorol.*, *5*(5), 763–773.
Nakai, Y., H. Kitahara, and T. Saito (1994), Snow interception by forest canopies: Weighing a conifer tree, meteorological observation and analysis by the Penman-Montheith formula, in *Proceedings of Yokohama Symposia J2 and J5 on Snow and Ice Covers: Interactions with the Atmosphere and Ecosystems*, vol. 223, pp. 227–236, Yokohama, Japan.
Nakai, Y., T. Sakamoto, T. Terajima, K. Kitamura, and T. Shirai (1999), Energy balance above a boreal coniferous forest: A difference in turbulent fluxes between snow-covered and snow-free canopies, *Hydrol. Processes*, *13*(4), 515–529.
Oleson, K., D. Lawrence, G. Bonan, and M. Flanner (2010), *Technical Description of Version 4.0 of the Community Land Model (CLM)*, Natl. Cent. for Atmos. Res., Clim., and Global Dyn. Div., Boulder, Colo.
Pomeroy, J., and D. M. Gray (1995), Snowcover: Accumulation, relocation, and management, *NHRI Sci. Rep.7*, Saskatoon, Sask., Canada, Environment Canada.
Pomeroy, J., J. Parviainen, N. R. Hedstrom, and D. M. Gray (1998), Coupled modelling of forest snow interception and sublimation, *Hydrol. Processes*, *12*, 2317–2337.
Pomeroy, J., N. R. Hedstrom, and J. Parviainen (1999), *The Snow Mass Balance of Wolf Creek, Wolf Creek Research Basin: Hydrology, Ecology, Environment*. Natl. Water Res. Inst., Environ. Can., Saskatoon, Sask.
Roesch, A. (2006), Evaluation of surface albedo and snow cover in AR4 coupled climate models, *J. Geophys. Res.*, *111*, D15111, doi:10.1029/2005JD006473.
Rohrer, M. D. (1989), Determination of the transition air temperature from snow and rain and intensity of precipitation, in *IAHS/WMO/ETH International Workshop of Precipitation Measurement*, edited by B. Sevruk, pp. 475–482, World Meteorological Organization.
Rutter, N., R. Essery, J. Pomeroy, N. Altimir, K. Andreadis, I. Baker, A. Barr, and P. Bartlett (2009), Evaluation of forest snow processes models (SnowMIP2), *J. Geophys. Res.*, *114*, D06111, doi:10.1029/2008JD011063.
Satterlund, D., and H. Haupt (1967), Snow catch by conifer crowns, *Water Resour. Res.*, *3*(4), 1035–1039.
Schleppi, P., M. Conedera, I. Sedivy, A. Thimonier, 2007. Correcting non-linearity and slope effects in the estimation of the leaf area index of forests from hemispherical photographs, *Agric. For. Meteorol.*, *144*(3–4), 236–242.
Schmidt, R. A. (1991), Sublimation of snow intercepted by an artificial conifer, *Agric. For. Meteorol.*, *144*(3–4), 236–242.
Schmidt, R. A., and D. Gluns (1991), Snowfall interception on branches of three conifer species, *Can. J. For. Res.*, *21*, 1262–1269.
Shidei T, T. Takahashi, K. Takahashi and K. Kataoka (1952), Study of the fallen snow on the forest trees, *Bull. Gov. For. Exp. Stn.*, *54*, 115–164.
Storck, P. (2000), Trees, snow and flooding: An investigation of forest canopy effects on snow accumulation and melt at the plot and watershed scales in the Pacific northwest, *Tech. Rep. 161*, 195 pp., Univ. of Wash., Seattle. [Available at http://www.ce.washington.edu/pub/WRS/WRS161.pdf.]
Storck, P., D. P. Lettenmaier, and S. M. Bolton (2002), Measurement of snow interception and canopy effects on snow accumulation and melt in a mountainous maritime climate, Oregon, United States, *Water Resour. Res.*, *38*(11), 1223, doi:10.1029/2002WR001281.
Strasser, U., J. Corripio, F. Pellicciotti, P. Burlando, B. Brock, and M. Funk (2004), Spatial and temporal variability of meteorological variables at Haut Glacier d'Arolla (Switzerland) during the ablation season 2001: Measurements and simulations, *J. Geophys. Res.*, *109*, D03103, doi:10.1029/2003JD003973.
Strasser, U., M. Bernhardt, M. Weber, G. E. Liston, and W. Mauser (2008a), Is snow sublimation important in the alpine water balance?, *The Cryosphere*, (2), 53–66.
Strasser, U., J. Corripio, B. Brock, F. Pellicciotti, and P. Burlando (2008b), Distributed modeling of snow processes in The Berchtesgaden National Park, in *Alpine Snow Workshop*, edited by U. Strasser, Berchtesgaden Natl. Park, Munich, Germany.
Suzuki, K., and Y. Nakai (2008), Canopy snow influence on water and energy balances in a coniferous forest plantation in northern Japan, *J. Hydrol.*, *352*(1–2), 126–138.
Tarboton, D. G., and C. H. Luce (1996), *Utah Energy Balance Snow Accumulation and Melt Model (UEB). Computer Model Technical Description and Users Guide*, Utah Water Res. Lab. and USDA For. Serv. Intermountain Res. Stn., Fort Collins, Colo.
Tennyson, L., F. Ffolliott, and D. Thorud (1974), Use of time lapse photography to assess potential interception in Arizona ponderosa pine, *Water Resour. Bull.*, *10*(6), 1246–1254.
Thimonier, A., I. Sedivy, and P. Schleppi (2010), Estimating leaf area index in different types of mature forest stands in Switzerland: A comparison of methods, *Eur. J. For. Res.*, *129*(4), 543–562.
Troendle, C. A., and J. R. Meiman (1986), The effect of patch clear cutting on the Water Balance of a Subalpine Forest Slope, Proceedings of the 54th Annual Western Snow Conference, Phoenix Arizona, Fort Collins, Colo., pp. 93–100.
US Army Corps of Engineers (1956), *Snow Hydrology: Summary Report of the Snow Investigations*, pp. 437, North Pac. Div., Portland, Oreg.
Varhola, A., and N. C. Coops (2013), Estimation of watershed-level distributed forest structure metrics relevant to hydrologic modeling using LiDAR and Landsat, *J. Hydrol.*, *487*, 70–86.
Varhola, A., N. C. Coops, C. W. Bater, P. Teti, S. Boon, and M. Weiler (2010a), The influence of ground- and lidar-derived forest structure metrics on snow accumulation and ablation in disturbed forests, *Can. J. For. Res.*, *40*(4), 812–821.
Varhola, A., N. C. Coops, M. Weiler, and R. D. Moore (2010b), Forest canopy effects on snow accumulation and ablation: An integrative review of empirical results, *J. Hydrol.*, *392*(3–4), 219–233.
Veatch, W., P. D. Brooks, J. R. Gustafson, and N. P. Molotch (2009), Quantifying the effects of forest canopy cover on net snow accumulation at a continental, mid-latitude site, *Ecohydrology*, *2*(2), 115–128.
Verseghy, D. (1990), CLASS—A Canadian land surface scheme for GCMS. I. Soil model, *Int. J. Climatol.*, *11*, 111–133.

Wever, N., C. Fierz, C. Mitterer, H. Hirashima, and M. Lehning (2014), Solving richards equation for snow improves snowpack meltwater runoff estimations in detailed multi-layer snowpack model, *Cryosphere*, *8*(1), 257–274.

Wilm, H., and E. Dunford (1945), *Effect of Timber Cutting on Water Available for Streamflow From a Lodgepole Pine*, U. S. Dep. of Agric., Washington, D. C.

Winkler, R. D., and R. D. Moore (2006), Variability in snow accumulation patterns within forest stands on the interior plateau of British Columbia, Canada, *Hydrol. Processes*, *20*(17), 3683–3695.

Winkler, R. D., D. L. Spittlehouse, and D. L. Golding (2005), Measured differences in snow accumulation and melt among clearcut, juvenile, and mature forests in southern British Columbia, *Hydrol. Processes*, *19*(1), 51–62.

Ye, H., J. Cohen, and M. Rawlins (2013), Discrimination of solid from liquid precipitation over Northern Eurasia using surface atmospheric conditions, *J. Hydrometeorol.*, *14*, 1345–1355.